

www.acsami.org Research Article

Vat Photopolymerization of Reinforced Styrene-Butadiene Elastomers: A Degradable Scaffold Approach

Christopher Kasprzak, James R. Brown, Keyton Feller, Philip J. Scott, Viswanath Meenakshisundaram, Chris Williams, and Timothy Long*



Cite This: ACS Appl. Mater. Interfaces 2022, 14, 18965–18973



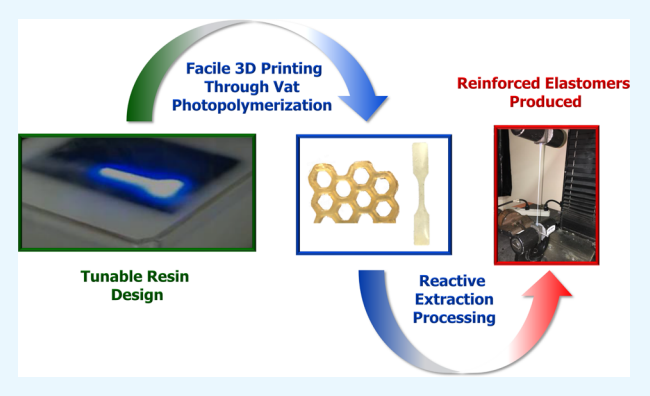
ACCESS

Metrics & More

Article Recommendations

s Supporting Information

ABSTRACT: Vat photopolymerization (VP) is a high-throughput additive manufacturing modality that also offers exceptional feature resolution and surface finish; however, the process is constrained by a limited selection of processable photocurable resins. Low resin viscosity (<10 Pa·s) is one of the most stringent process-induced constraints on resin processability, which in turn limits the mechanical performance of printed resin systems. Recently, the authors created a VP-processable photosensitive latex resin, where compartmentalization of the high molecular weight polymer chains into discrete particles resulted in the decoupling of viscosity from molecular weight. However, the monomers used to form the hydrogel green body resulted in decreased ultimate material properties due to the high cross-link density. Herein, we report a novel scaffold that



allows for facile UV-based AM and simultaneously enhances the final part's material properties. This is achieved with a chemically labile acetal-containing cross-linker in conjunction with N-vinylpyrrolidone, which forms a glassy polymer after photocuring. Subsequent reactive extraction cleaves the cross-links and liberates the glassy polymer, which provides mechanical reinforcement of the geometrically complex VP-printed elastomer. With only a 0.1 wt % loading of photoinitiator, G'/G'' crossover times of less than 1 s and green body plateau moduli nearing 10^5 Pa are obtained. In addition, removal of the hydrophilic and thermally labile scaffold results in decreased water uptake and increased thermal stability of the final printed part. Ultimate strain and stress values of over 650% and 8.5 MPa, respectively, are achieved, setting a new benchmark for styrene—butadiene VP elastomers.

KEYWORDS: vat photopolymerization, reinforced elastomer, reactive extraction, latex, acetal, scaffold

1. INTRODUCTION

Vat photopolymerization (VP) is a high-throughput additive manufacturing modality for 3D printing photocurable polymeric materials. VP provides superb surface resolution and feature resolution, allowing for micron-scale control of photocured geometries. 1-3 However, the process imposes certain limitations on photopolymer design. Specifically, the recoating process performed between printing of each layer requires a resin viscosity of $\sim \le 10 \text{ Pa} \times \text{s}$, which limits the molecular weight of photopolymers to monomers and oligomers due to the power law dependence of solution and melt viscosity with respect to polymer molecular weight.⁶⁻⁹ In addition, each photocured layer must possess sufficient mechanical strength to resist the shear forces of recoating, support subsequent printed layers, and maintain part shape and integrity. High cross-link densities are often employed in VP to impart the necessary strength to the green body, which are typically correlated to a shear modulus on the order of 10⁴–10⁶ Pa. ^{10,11} However, materials possessing high cross-link densities exhibit low molecular weight between cross-links (M_c) . The use of low molecular weight precursors in VP resins

results in brittle behavior, as satisfactory elastomeric properties are typically obtained through cross-linking preformed high molecular weight polymers, which provides a higher $M_{\rm c}$. Thus, a seemingly insurmountable compromise arises, that is, to achieve facile printing, the final material must exhibit low ultimate strain due to the trade-off between resin viscosity and cross-link density.

Recently, our group developed a VP resin design approach to mitigate the compromises traditionally imposed with regards to printability versus final material properties. Our laboratories dissolved photoactive monomers into the aqueous phase of a styrene—butadiene rubber (SBR) latex to generate a photosensitive low viscosity resin. The decoupling of viscosity from molecular weight afforded by sequestration of high

Received: February 24, 2022 Accepted: April 11, 2022 Published: April 14, 2022





molecular weight polymer chains into discrete nanoparticles provided the basis for the low viscosity resin that exhibited high $M_{\rm c}$ after processing. Once VP generates a green body of the desired shape, the latex particles coalesce upon thermal treatment, forming a semi-interpenetrating network. This process resulted in excellent elastomeric properties, setting a new benchmark for additive manufacturing of SBR-based elastomers of 500% ultimate strain and 5 MPa ultimate stress.

While VP provides access to novel architectures, combining this printing modality with nanotechnology creates an opportunity for advanced material development with regards to tailored polymer nanocomposites. Polymer nanocomposites continue to fascinate the scientific community, generating tens of thousands of citations in 2020 alone. Carbon nanotubes, ^{12,13} graphene, ¹⁴ silica, ¹⁵⁻¹⁷ titanium dioxide, ¹⁸ cobalt, ¹⁹ gold, ^{20,21} and clay ²²⁻²⁴ represent only a subset of the vast array of inorganic nanomaterials utilized in these composites. Organic nanomaterials such as cellulose, 25,26 chitin and chitosan, 27 and synthetic polymers²⁸ continue to sculpt the future of materials research as well. These nanomaterials impart beneficial properties such as molecular sensing capabilities, ^{21,29,30} increased membrane selectivity, ^{31–33} and enhanced mechanical behavior. 17,28,34-36 In 2020, our group described a process for fabricating UV-assisted direct ink write (UV-DIW) parts from a hybrid colloid resin resulting in a mechanically reinforced silica-SBR nanocomposite. This work demonstrated the tremendous promise of merging the vast nanocomposite literature with cutting-edge additive manufacturing techniques.¹⁷

Photopolymerizable scaffolds continue to find novel uses in additive manufacturing; however, no examples exist of *in situ* generation of favorable components such as mechanical reinforcing agents.^{37–39} For example, Zou et al. dissolved a 3D printed porous poly(vinyl alcohol) scaffold after filling the structure with a bioink formulation, giving rise to a microfluidic channel network architecture.⁴⁰ Conversely, Park et al. generated porous structures through extrusion of polycaprolactone and poly(ethylene glycol) (PEG) followed with subsequent dissolution of the PEG to generate the micropores.⁴¹ Herzberger et al. and Hegde et al. employed VP to fabricate complex parts composed of all-aromatic polyimides after thermal removal of the photopolymerized scaffold.^{10,42} In all of these studies, the scaffold only served as a sacrificial template for the final part geometry.

In this work, we challenge the paradigm that the scaffold serves only as a sacrificial material. Instead, we design it to both template the desired final geometry as well as impart beneficial mechanical properties. Careful synthetic design facilitated implementation of an acid-labile scaffold composed of acetalcontaining PEG cross-links with glassy polyvinylpyrrolidone (PVP). Judicious monomer and photoinitiator selection allowed for generation of a photosensitive SBR latex resin that demonstrated colloidal stability and possessed appropriate curing kinetics, green body strength, and viscosity suitable for VP processing. Coalescence of the latex particles throughout the swollen hydrogel formed through VP generated a robust elastomeric part; however, the presence of the cross-linked scaffold limited the ultimate mechanical properties obtained. Reactive extraction of the VP part cleaved the labile cross-links and resulted in a mechanically reinforced elastomeric nanocomposite exhibiting superb mechanical properties.

2. MATERIALS AND METHODS

2.1. Materials. Styrene-butadiene rubber (SBR) latex (Rovene 4176) was generously donated by Mallard Creek Polymers Inc. The solids content of this latex was 50 wt %, with a particle diameter range of 120-170 nm, and a viscosity of 400 cps as reported by the manufacturer. The SBR copolymer was approximately 50/50 by weight styrene and butadiene with a low level of carboxylic acid monomer incorporated into the polymer and neutralized with ammonia to enhance colloidal stability. The polymer contains a high insoluble (gel) content from the polymerization process due to intraparticle cross-linking during the polymerization process. 1-Vinyl-2-pyrrolidinone (NVP) and poly(ethylene glycol) diacrylate (PEGDA 575, 575 g/mol), poly(ethylene glycol) (PEG 300, 300 g/mol) dimethyl phenylphosphonite, 2,4,6-trimethylbenzoyl chloride, lithium bromide (LiBr), 2-butanone, calcium hydride (CaH₂), magnesium sulfate (MgSO₄), sodium bicarbonate (NaHCO₃), para-toluenesulfonic acid monohydrate (p-TSA) 98.5%, (1S)-(+)-10-camphorsulfonic acid (CSA), ethylene glycol monovinyl ether, acryloyl chloride, and diphenyl(2,4,6-trimethylbenzoyl)phosphine oxide (TPO) were purchased from Millipore Sigma and used as received.

2.2. Methods. 2.2.1. Synthesis of Water-Soluble Photoinitiator. A lithium acylphosphinate salt (LAP) was synthesized according to prior literature. 43,44 In short, 2,4,6-trimethylbenzoyl chloride was added dropwise to stirring dimethyl phenylphosphonite in an equimolar amount under argon at 25 °C. The mixture was stirred for 18 h, and then LiBr (4 equiv) dissolved in 2-butanone was added to the reaction and heated to 50 °C. After 10 min, the mixture was cooled to 25 °C and stirred for 4 h. The resulting mixture was filtered and washed with 2-butanone, then dried at 25 °C under vacuum.

2.2.2. Synthesis of Chemically Labile Cross-linker. Poly(ethylene glycol) diacetal diacrylate 586 g/mol (PEGdAdAc) was synthesized according to prior literature. First, monovinyl ether ethylene glycol acrylate was synthesized according to the procedure detailed by Jiang et al. Then PEG 300 was dissolved in dichloromethane (DCM) and stirred over molecular sieves with monovinyl ether ethylene glycol acrylate (2.2 equiv). The solution was chilled to 0 °C prior to the addition of p-TSA (0.125 equiv) dissolved in THF. The reaction was allowed to proceed for 50 min before quenching with saturated aqueous NaHCO₃ solution. The resulting solution was extracted with DCM three times. Then the organic layers were combined and dried over MgSO₄, filtered, and concentrated through rotary evaporation until dry.

2.2.3. Photocurable Latex Preparation. Photocurable latex formulations containing TPO were prepared as described in our previous work. For LAP containing formulations, a standard example (4:1 SBR:scaffold, 1:1 PEGdAdAc:NVP (wt:wt)) is as follows. Twenty milligrams of LAP was added to a 30 mL vial containing 20 g of latex equipped with a stir bar. The vial was covered in aluminum foil to minimize ambient light and vortexed to dissolve the LAP. In a separate vial, 1.2 g of each scaffold monomer was added and vortexed. The scaffold monomer mixture was added dropwise to the latex under rapid stirring. The entire system was vortexed for 30 s after addition was completed.

2.2.4. Analytical Methods. Differential scanning calorimetry (DSC) was performed at 50 mL min⁻¹ N₂ flow rate with a 10 °C min⁻¹ heating rate, and 80 °C min⁻¹ cooling rate on a TA Instruments Q2000 equipped with a RCS 90 cooling system. The glass transition (T_g) values were determined using the universal analysis software to measure the midpoint of the endothermic transition on the second heating cycle. TGA was performed on a TA Instruments Q500 under N₂ atmosphere with a 15 min isotherm at 100 °C and a 10 °C min⁻¹ ramp from 100 to 600 °C. ¹H NMR spectroscopy in D₂O on a Varian Unity 400 MHz confirmed the chemical structure of synthesized materials. Tensile experiments were executed on an Instron 5500R tensile tester at a strain rate of 50 mm min⁻¹ at ambient temperature. Tensile specimens were fabricated according to the procedure detailed in our previous publication.⁵ Photorheology was performed on a TA Instruments DHR-2 equipped with a SmartSwap UV assembly with 20 mm aluminum upper plate,

20 mm quartz lower plate, and Omnicure S2000 high-pressure mercury light source (320-500 nm filter). UV intensity was measured with a Silverline radiometer and 20 mm sensor attachment for the quartz parallel plate. Data were gathered at a 500 μ m gap, 0.2% strain, and 1 Hz. UV radiation was applied at an intensity 250 mW/cm² for 120 s after a 30 s delay. The rheometer was set to maintain 0 N axial force within a ±1 N tolerance through slight adjustments in gap size. Samples were run under air without purge of inert gas. All samples were run in triplicate to ensure consistency and reproducibility of this technique. Plateau storage moduli values were calculated from the last 20 s of the G' curve; moduli crossover (G'/G'') values were determined using the dedicated feature in TA Instruments TRIOS software. Gel fractions were determined as the difference in dry weight before and after 24 h extraction and averaged over three replicates.

2.2.5. Water Uptake Determination. Materials were dried at 70 °C under vacuum for 24 h prior to analysis. Upon removal from the vacuum oven, the samples were sealed in dried vials and then transferred and loaded into a TA Instruments TGA-SA Q5000. A given sample was then dried within the instrument at 60 °C and 0% relative humidity (R.H.) for 1 h prior to a 450 min isohume at 95% R.H. and 25 °C. The final water uptake value is reported.

2.2.6. Scaffold Removal Quantification. A 1 L beaker equipped with a stir bar covered with a grate was filled with 1 L of 0.05 M CSA in CHCl₃-IPA solution and capped with a glass plate. The CHCl₃:IPA was varied from 0:100 to 50:50 (V/V%). Materials were submerged in the acidic solution for 24 h at 50 °C under mild stirring. Then the reactively extracted materials were submerged in a neutral CHCl3-IPA solution for 4 h, then washed with neutral CHCl3-IPA solution and thoroughly washed with DI water. Finally the samples were dried at 70 °C under vacuum for 24 h prior to analysis. Scaffold removal was quantified gravimetrically as the difference in dry weight before and after the extraction procedure, accounting for the previously determined gel fraction. Pure latex elastomeric films demonstrated less than 1 wt % weight loss when subjected to the same reactive extraction procedure.

2.2.7. Vat Photopolymerization of Photocurable Formulations. The 3D printed specimens were fabricated with a custom-built vat photopolymerization AM system equipped with a high-resolution projector composed of a 1080p Texas Instrument digital micromirror device (DMD; 0.65"). UV exposure on the resin surface was grayscaled using the DMD to compensate for the colloidal resin scattering the UV irradiation, as detailed in our previous work. The projector is illuminated with a Dymax Bluewave 75 spot-cure lamp with an emission range from 350 to 500 nm. The maximum projected intensity is estimated at 22 mW/cm². DLIinnovations-DLP6500 optics create a projection size of $61 \times 34 \text{ mm}^2$, and a pixel size of 31 μ m. All specimens were exposed for 30 s/layer.

3. RESULTS AND DISCUSSION

Our laboratories pioneered the vat photopolymerization (VP) of high molecular weight polymers through compartmentalization of the polymer chains into discrete nanoparticles, which allowed for a low viscosity medium suitable for VP involving a recoating step. 46 Subsequent dissolution of photoactive monomers into the aqueous phase provided the necessary photosensitivity.⁵ This photoactive latex formulation provided a platform for generation of complex geometric structures composed of tough elastomeric material exceeding 500% ultimate strain and 5 MPa ultimate stress. However, the retention of the hydrophilic scaffold formed through the polymerization of the photoactive monomers resulted in unfavorable hygroscopicity. In addition, the cross-link density of the photopolymerized scaffold expressed a direct relationship with the storage modulus of the green body but demonstrated an inverse relationship with the ultimate strain exhibited by the final material. Generation of a green body with

sufficient strength to survive the recoating process involved in VP required a high scaffold cross-link density, yet a low scaffold cross-link density was desired to achieve greater elastomeric properties. This inspired the work described herein, where the results obtained from performing a reactive extraction procedure on a system using a chemically labile acetal-containing cross-linker, shown in Figure 1a, are detailed.

$$(a) \qquad (b) \qquad (b) \qquad (c) \qquad (d) \qquad (d) \qquad (d)$$

Figure 1. Chemical structures of scaffold monomers and photoinitiators used in this study (a) poly(ethylene glycol) diacetal diacrylate (PEGdAdAc) with acetal linkages highlighted in green, (b) NVP, (c) TPO, and (d) LAP.

In previous studies, an intermediate monomer ratio of 1:2.5 (wt:wt) of cross-linker (PEGDA) to NVP provided sufficient mechanical integrity to the green body to allow for printing while still allowing for greater than 500% ultimate strain in the final material. The inspiration to use a chemically labile crosslinker arose from the aforementioned compromise between printability and final material properties. We hypothesized that using a chemically labile cross-linker would allow for both facile manufacturing as well as provide desirable final material properties. A high cross-link density scaffold would template the geometry during VP, and then the selective cleavage of the acetal-containing cross-links in a postprocessing step would impart increased ultimate strain. The effect of cross-link density on the shear storage modulus (G') of the green body was deduced through photorheology, and the results are displayed below in Figure 2a. Using the previously optimized ratio of 1:2.5 PEGdAdAc:NVP resulted in a plateau modulus $\sim 10^4$ Pa; however, using the newly viable ratio of 1:1 PEGdAdAc:NVP resulted in a plateau modulus nearly an order of magnitude greater. This correlates to more facile manufacturing with regards to VP, as the printed hydrogels are more robust to layer recoating and to handling during postprocess removal and cleaning.

To increase the shelf life and impart consistent photosensitivity to the photoactive formulation, the legacy photoinitiator (PI) TPO was replaced with a previously reported water-soluble analog, LAP. The successful synthesis of LAP, confirmed through ¹H, ¹³C, and ³¹P NMR spectroscopy, provided a pure compound capable of initiating the photopolymerization of vinyl compounds (Scheme S1 and Figures S1-S3). However, LAP is a salt and it is well-known that the addition of salt to aqueous medium decreases the Debye length. 48-50 As the latex of interest is an electrostatically stabilized colloid, decreasing the Debye length may result in destabilization of the colloid through screening of repulsive electrostatic interactions and cause premature aggregation of the particles. The manifestation of this phenomenon is visible in Figure 2c and d, where a loading of 0.1 wt % LAP provided in a homogeneous and translucent film. On the contrary, a loading of 1.0 wt % LAP resulted in a heterogeneous and

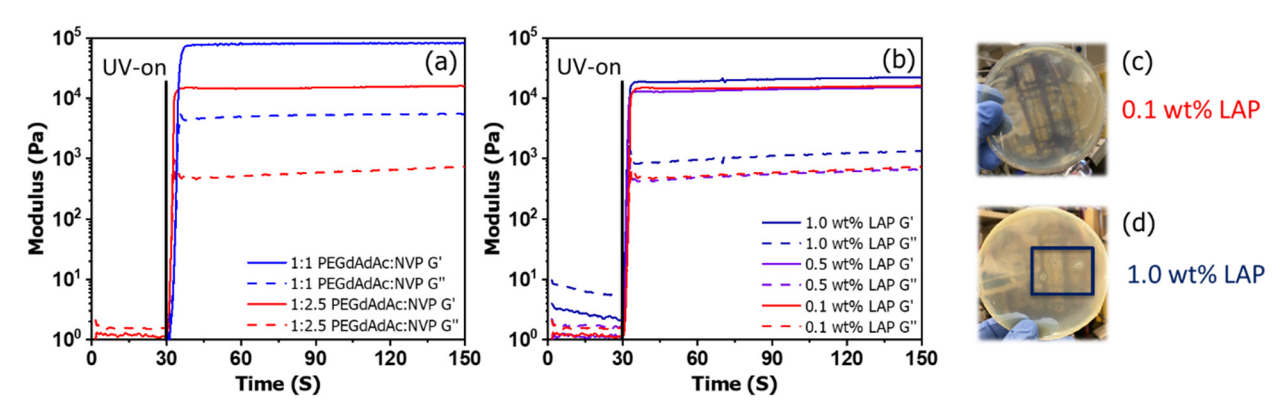


Figure 2. Photorheological profiles of photocurable latex formulations with (a) variable cross-linker concentration and (b) variable photoinitiator loading with corresponding pictures for (c) 0.1 wt % LAP loading and (d) 1.0 wt % LAP loading.

opaque film. Photorheological analysis over an order of magnitude range of PI loading deduced that a loading of 0.1 wt % LAP would not only maintain colloidal stability but also provide extremely fast crossover times of \sim 1 s and gel fractions near 90 wt %. These characteristics detailed in Table 1 are quite favorable for VP manufacturing.

Table 1. Summary of Photorheological Data and Gel Fractions of Photopolymerized Films Containing Variable Cross-linker and PI Loadings

PEGdAdAc:NVP	LAP content (wt %)	crossover time G'/G'' (s $\pm \sigma$)	plateau modulus ^a (kPa $\pm \sigma$)	gel fraction ^b (wt %)
1:1	0.1	1.0 ± 0.5	81 ± 3	91
1:2.5	0.1	1.0 ± 0.5	16 ± 1	90
1:2.5	0.5	1.0 ± 0.5	18 ± 4	89
1:2.5	1.0	1.0 + 0.5	20 + 1	90

^aDetermined through parallel plate photorheology. ^bDetermined through 24 h Soxhlet extraction in tetrahydrofuran.

Scaffold degradation requires additional composition and postprocessing method design beyond the requirements of photocurability. After extensive screening, a solution of 0.05 M (1S)-(+)-10-camphorsulfonic acid (CSA) in IPA and CHCl₃ demonstrated the most promising results, which are shown in Figure 3. Systematically varying the ratio of IPA:CHCl₃ v/v

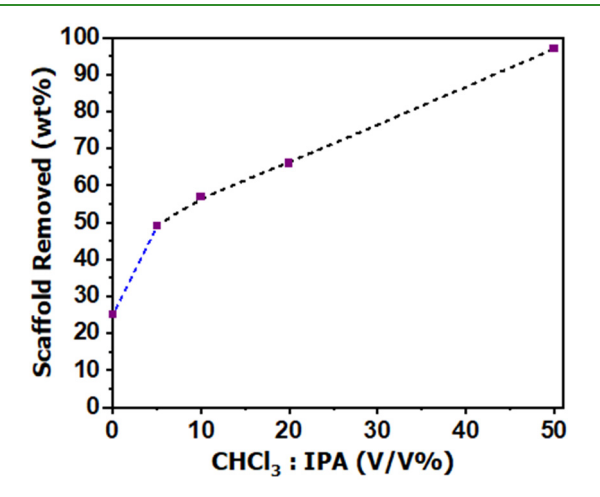
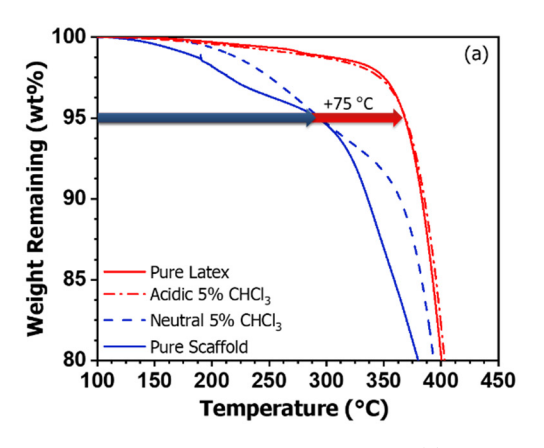


Figure 3. Chloroform content of acidic reactive extraction medium dictates magnitude of scaffold removal.

enabled an optimized degree of part swelling to facilitate extraction without damaging the printed geometry. While a 50:50 v/v IPA:CHCl₃ reactive extraction medium resulted in near quantitative removal of the scaffold, the medium swelled the elastomer drastically and ruptured the material. Conversely, a 95–5 v/v IPA-CHCl₃ solution swelled the material minimally, thus preserving geometric complexity and material integrity while enabling efficient extraction throughout the part. Thus, the 95:5 v/v IPA:CHCl₃ medium was chosen for subsequent studies.

Figure 4a depicts the thermogravimetric profiles from subjecting the materials to varying extraction conditions. Fabrication of the pure scaffold was performed through curing NVP and PEGdAdAc with a 1:1 w/w ratio, in the absence of the latex, and extracting the resulting polymer with a neutral 95:5 v/v IPA:CHCl₃ solution. Fabrication of the pure latex was performed through casting a film of the latex directly obtained from the manufacturer and extracting the polymer with a neutral 95:5 v/v IPA:CHCl3 solution. Fabrication of the VP elastomers subjected to neutral and acidic extractions is described in the experimental section. It is clearly shown that the acetal-containing scaffold displays a much lower degradation temperature, exhibiting a $T_{\rm d,5\%}$ 75 °C lower than the pure latex elastomer. This is consistent with previous studies of acetal-containing homopolymers, which lose over 70% of their mass when subjected to a 230 °C isotherm. 51 After extraction with acidic medium, the thermogravimetric profile of the VP elastomer shifted to overlay completely with the pure latex elastomer, thus demonstrating successful removal of the acetalcontaining portions of the polymer. DSC analysis of the polymers demonstrated a single $T_{\rm g}$ at -24 °C, supporting the claim that there is no significant phase mixing between the scaffold and latex elastomer or chemical modification of the elastomer due to the reactive extraction process.

Retaining the hydrophilic scaffold in the VP elastomer resulted in an increased tendency to absorb water from the air, or equivalently, hygroscopicity. Hygroscopicity is often unfavorable in VP parts and industrial elastomers due to the resulting dependence of mechanical properties on humidity as well as dimensional changes due to swelling. The scaffold used in this work is quite hydrophilic; it demonstrates over 70 wt % water uptake water when subjected to a 95% R.H. isohume, shown in Figure 5a. Figure 5b demonstrates how a neutral extraction of the scaffold-containing elastomer resulted in water uptake intermediate to the pure scaffold and pure latex. However, after reactive extraction processing, the



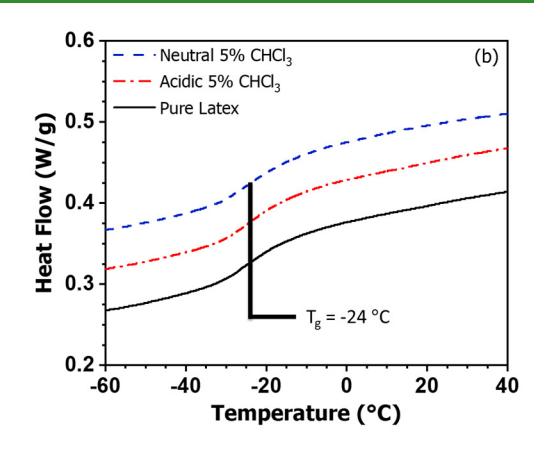
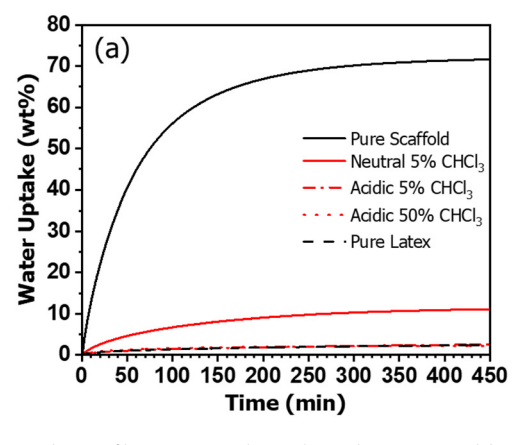


Figure 4. Thermal analysis of various elastomeric films. (a) Weight loss profiles obtained through TGA and (b) DSC thermograms with curves vertically shifted for clarity.



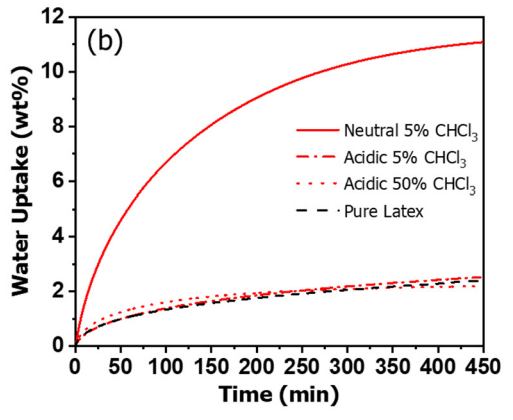


Figure 5. Water uptake profiles at 95% relative humidity measured by TGA-SA of the pure scaffold, pure latex, neutral extraction, and reactive extraction elastomeric films. (a) All materials and (b) excluding the pure scaffold for clarity.

elastomer water uptake profile collapses to the profile of the pure latex. This extraction process thus imparts greater water resistance to printed objects, with respect to mechanical properties and geometric fidelity, through decreased hygroscopicity.

Tensile analysis of the acid-extracted VP elastomer, displayed in Figure 6 and summarized in Table 2, demonstrated mechanical reinforcement when compared to the stress-strain profiles of the pure latex. The acid-extracted

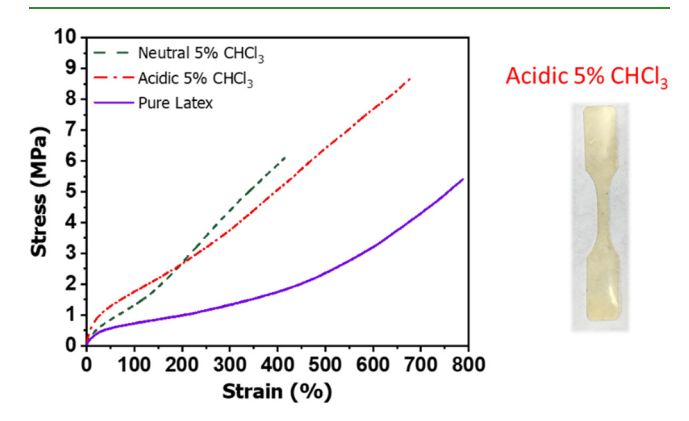


Figure 6. Stress-strain profiles of photopolymerized materials subjected to different extraction conditions as well as the pure latex, accompanied by a representative photo of a tensile specimen punched from the reactively extracted elastomeric film.

Table 2. Summary of Mechanical Properties Obtained through Tensile Analysis of Photopolymerized Materials Subjected to Different Extraction Conditions as Well as **Pure Latex**

sample	neutral 5% CHCl ₃	acidic 5% CHCl ₃	pure latex
ultimate strain (% $\pm \sigma$)	450 ± 30	670 ± 20	780 ± 90
ultimate stress (MPa $\pm \sigma$)	6.5 ± 0.6	8.5 ± 1.1	5.7 ± 0.3

VP elastomer averaged an ultimate strain of over 650% and an increase in ultimate stress of nearly 50% compared to the pure latex. This phenomenal ultimate strain coupled with a high ultimate stress provides a new benchmark for additively manufactured elastomers, surpassing previous state-of-the-art materials⁵ by 150% ultimate strain. The increase in stress is explained through considering the nature of the monomers used in the scaffold. The acid-cleavable acetal linkages in the cross-linker flank an oligomeric PEG species. Cleavage of the acetal linkage results in removal of the oligomeric PEG but allows for variable retention of the polymerized NVP dependent upon the extraction conditions. PVP is a glassy amorphous polymer under ambient conditions with a reported $T_{\rm g}$ ranging from 120 to 180 °C, ⁵⁴ and Hourston et al. demonstrated previously that glassy polymers act as reinforcing fillers in latex-based elastomers.2

To further confirm that the mechanical reinforcement is derived from a matrix-filler like interaction, investigations into

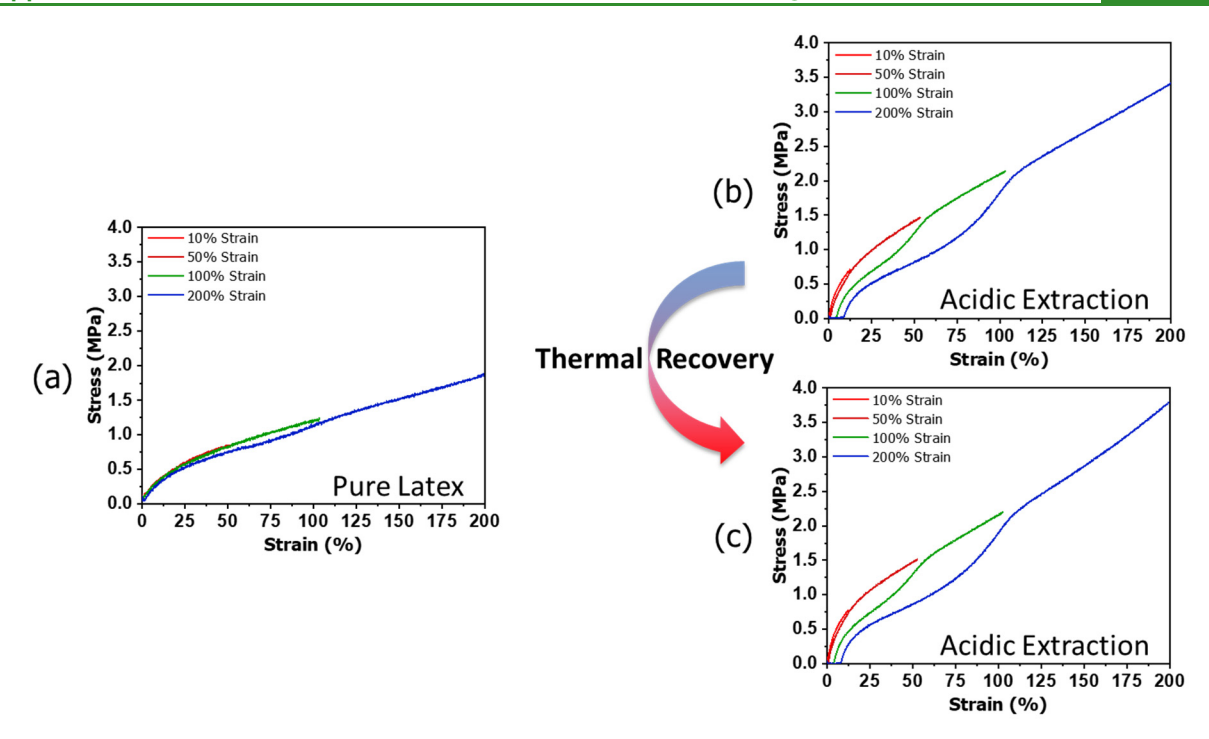
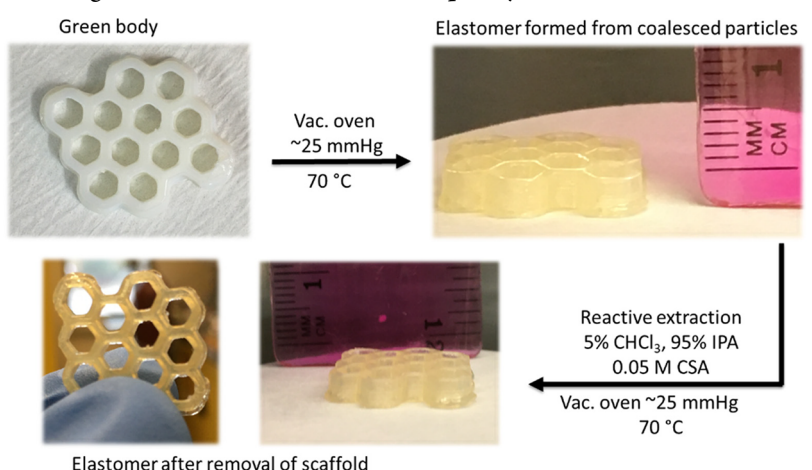


Figure 7. Stress-strain profiles of elastomeric materials subjected to successively increasing strain. (a) Pure latex, (b) reactively extracted VP material, and (c) exact same tensile specimen used in panel b after undergoing a thermal recovery process.

Scheme 1. Photographic Flowchart of Subjecting a Vat Photopolymerized Print to Particle Coalescence and Reactive Extraction Process Demonstrating Retention of Geometrical Complexity



the Mullins effect were performed. Figure 7a sets a baseline for these studies. The pure latex was subjected to successively increasing maximum strains with a 30 s rest at 0% strain between each subsequent cycle. The material demonstrated almost perfect overlap of stress-strain profiles for successively increasing strains. When considering Figure 7b, stress-softening is clearly observed. In other words, the acid-extracted VP elastomer displayed a lower stress at the same strain during subsequent strains. For example, the 200% strain test displayed a stress of 0.5 MPa at 25% strain, whereas the prior 50% strain test displayed 1 MPa stress at 25% strain. The stress-softening occurs to an extent where the material begins to overlay with the pure latex, demonstrating that the matrix begins dominating the mechanical properties. It is clear that there is an interaction between the filler and the matrix that is disturbed upon mechanical deformation, which is consistent

with the Mullins effect. 17,55 Figure 7c confirms that this phenomenon is of noncovalent origin, as a simple isothermal treatment at 70 °C for 24 h under reduced pressure causes the material to fully recover and the stress-softening phenomenon is observed again. As the thermal treatment is performed at a temperature far below the reported $T_{\rm g}$ of PVP, the stressrecovery is attributed to movement of the matrix polymer chains. It is worthy to note that the acid-extracted VP elastomer not only outperformed the neutral extraction by over 200% ultimate strain but also demonstrated over 30% increased ultimate stress. We postulate that liberation of the glassy PVP from the cross-linked scaffold results in enhanced matrix-filler interactions compared to the neutral extracted VP elastomer. However, detailed morphological investigations were outside the scope of this study and are the focus of future work.

The reactive extraction process not only generates reinforcing agents *in situ* for these VP elastomers but also allows for retention of geometric complexity, as shown in Scheme 1. First, a 3D part was fabricated from the photoactive resin through VP printing. Drying of the part results in coalescence of the latex particles throughout the hydrogel. Subsequent reactive extraction reduces hygroscopicity and improves mechanical properties through cross-link removal and reinforcing agent generation. The resulting AM part retains the resolution afforded through VP, thus demonstrating the viability of this novel photoactive resin for fabrication of geometrically complex reinforced SBR elastomers.

4. CONCLUSIONS

A novel photocurable and acid labile scaffold was used to fabricate geometrically complex parts through VP and yield mechanically reinforced SBR elastomers. These elastomers exhibited superb mechanical properties as demonstrated through ultimate strain and stress values over 650% and 8 MPa, respectively, setting a new benchmark for additively manufactured SBR-based elastomers. Synthetic design of water-soluble photopolymerizable monomers provided acid labile functionalities through incorporation of acetal linkages into the cross-linking agent. These acid labile connections were degraded through a reactive extraction process after coalescence of the latex particles throughout the photopolymerized hydrogel. This allowed for partial removal of the scaffold and decreased hygroscopicity of the VP elastomer while simultaneously facilitating in situ generation of mechanical reinforcing agents. Partial retainment of the scaffold in the final part resulted in an elastomeric nanocomposite and provided mechanical reinforcement due to the glassy nature of the photopolymer. Careful selection of the reactive extraction medium allowed for retention of geometrical complexity afforded by the VP process. This work represents the first to design a degradable scaffold system for additive manufacturing of elastomers that results in enhanced final material properties as opposed to the current paradigm that the scaffold serves only as a sacrificial material for geometry definition.

ASSOCIATED CONTENT

5 Supporting Information

The Supporting Information is available free of charge at https://pubs.acs.org/doi/10.1021/acsami.2c03410.

Synthetic method used for generation of LAP; ³¹P NMR spectroscopy of LAP; ¹³C NMR spectroscopy of LAP; ¹H NMR spectroscopy of LAP; entire TGA profile for materials shown in Figure 4a (PDF)

AUTHOR INFORMATION

Corresponding Author

Timothy Long — School of Molecular Sciences, Biodesign Center for Sustainable Macromolecular Materials and Manufacturing, Arizona State University, Tempe, Arizona 85281, United States; orcid.org/0000-0001-9515-5491; Email: Timothy.E.Long@asu.edu

Authors

Christopher Kasprzak – Macromolecules Innovation Institute (MII) and Department of Chemistry, Virginia Tech,

- Blacksburg, Virginia 24061, United States; oorcid.org/0000-0003-4061-4683
- James R. Brown School of Molecular Sciences, Biodesign Center for Sustainable Macromolecular Materials and Manufacturing, Arizona State University, Tempe, Arizona 85281, United States
- Keyton Feller Macromolecules Innovation Institute (MII) and Department of Mechanical Engineering, Virginia Tech, Blacksburg, Virginia 24061, United States; ocid.org/0000-0001-7972-149X
- Philip J. Scott Macromolecules Innovation Institute (MII) and Department of Chemistry, Virginia Tech, Blacksburg, Virginia 24061, United States; orcid.org/0000-0002-4219-6000
- Viswanath Meenakshisundaram Macromolecules Innovation Institute (MII) and Department of Mechanical Engineering, Virginia Tech, Blacksburg, Virginia 24061, United States
- Chris Williams Macromolecules Innovation Institute (MII) and Department of Mechanical Engineering, Virginia Tech, Blacksburg, Virginia 24061, United States

Complete contact information is available at: https://pubs.acs.org/10.1021/acsami.2c03410

Funding

This work was funded by the National Science Foundation (NSF) GOALI grant in partnership with Michelin (CMMI–1762712).

Notes

The authors declare no competing financial interest.

REFERENCES

- (1) Appuhamillage, G. A.; Chartrain, N.; Meenakshisundaram, V.; Feller, K. D.; Williams, C. B.; Long, T. E. 110th Anniversary: Vat Photopolymerization-Based Additive Manufacturing: Current Trends and Future Directions in Materials Design. *Ind. Eng. Chem. Res.* **2019**, *58*, 15109–15118.
- (2) Thrasher, C. J.; Schwartz, J. J.; Boydston, A. J. Modular Elastomer Photoresins for Digital Light Processing Additive Manufacturing. ACS Appl. Mater. Interfaces 2017, 9, 39708–39716.
- (3) Zhang, F.; Zhu, L.; Li, Z.; Wang, S.; Shi, J.; Tang, W.; Li, N.; Yang, J. The Recent Development of Vat Photopolymerization: A Review. *Addit. Manuf.* **2021**, *48*, 102423.
- (4) Halloran, J. W. Ceramic Stereolithography: Additive Manufacturing for Ceramics by Photopolymerization. *Annu. Rev. Mater. Res.* **2016**, *46*, 19–40.
- (5) Scott, P. J.; Meenakshisundaram, V.; Hegde, M.; Kasprzak, C. R.; Winkler, C. R.; Feller, K. D.; Williams, C. B.; Long, T. E. 3D Printing Latex: A Route to Complex Geometries of High Molecular Weight Polymers. *ACS Appl. Mater. Interfaces* **2020**, *12*, 10918–10928.
- (6) Rau, D. A.; Forgiarini, M.; Williams, C. B. Hybridizing Direct Ink Write and Mask-Projection Vat Photopolymerization to Enable Additive Manufacturing of High Viscosity Photopolymer Resins. *Addit. Manuf.* 2021, 42, 101996.
- (7) Rubinstein, M.; Colby, R. *Polymer Physics*, 1st ed.; Oxford University Press: Oxford, NY, 2003.
- (8) Al Rashid, A.; Ahmed, W.; Khalid, M. Y.; Koç, M. Vat Photopolymerization of Polymers and Polymer Composites: Processes and Applications. *Addit. Manuf.* **2021**, *47*, 102279.
- (9) Colby, R. H.; Fetters, L. J.; Graessley, W. W. Melt Viscosity-Molecular Weight Relationship for Linear Polymers. *Macromolecules* 1987, 20, 2226–2237.
- (10) Hegde, M.; Meenakshisundaram, V.; Chartrain, N.; Sekhar, S.; Tafti, D.; Williams, C. B.; Long, T. E. 3D Printing All-Aromatic

- Polyimides Using Mask-Projection Stereolithography: Processing the Nonprocessable. *Adv. Mater.* **2017**, *29*, 1701240.
- (11) Sirrine, J. M.; Meenakshisundaram, V.; Moon, N. G.; Scott, P. J.; Mondschein, R. J.; Weiseman, T. F.; Williams, C. B.; Long, T. E. Functional Siloxanes with Photo-Activated, Simultaneous Chain Extension and Crosslinking for Lithography-Based 3D Printing. *Polymer* **2018**, *152*, 25–34.
- (12) Kasprzak, C. R.; Scherzinger, E. T.; Sarkar, A.; Miao, M.; Porcincula, D. H.; Madriz, A. M.; Pennewell, Z. M.; Chau, S. S.; Fernando, R.; Stefik, M.; Zhang, S. Ordered Nanostructures of Carbon Nanotube-Polymer Composites from Lyotropic Liquid Crystal Templating. *Macromol. Chem. Phys.* **2018**, *219*, 1800197.
- (13) Tomal, W.; Krok, D.; Chachaj-Brekiesz, A.; Lepcio, P.; Ortyl, J. Harnessing Light to Create Functional, Three-Dimensional Polymeric Materials: Multitasking Initiation Systems as the Critical Key to Success. *Addit. Manuf.* **2021**, *48*, 102447.
- (14) Prosheva, M.; Aboudzadeh, M. A.; Leal, G. P.; Gilev, J. B.; Tomovska, R. High-Performance UV Protective Waterborne Polymer Coatings Based on Hybrid Graphene/Carbon Nanotube Radicals Scavenging Filler. *Part. Part. Syst. Charact.* **2019**, *36*, 1800555.
- (15) Bourgeat-Lami, E.; Espiard, P.; Guyot, A. Poly(Ethyl Acrylate) Latexes Encapsulating Nanoparticles of Silica: 1. Functionalization and Dispersion of Silica. Polymer 1995, 36, 4385–4389.
- (16) Hu, J.; Chen, M.; Wu, L. Organic-Inorganic Nanocomposites Synthesized Viaminiemulsion Polymerization. *Polym. Chem.* **2011**, *2*, 760–772
- (17) Scott, P. J.; Rau, D. A.; Wen, J.; Nguyen, M.; Kasprzak, C. R.; Williams, C. B.; Long, T. E. Polymer-Inorganic Hybrid Colloids for Ultraviolet-Assisted Direct Ink Write of Polymer Nanocomposites. *Addit. Manuf.* **2020**, *35*, 101393.
- (18) Anirudhan, T. S.; Christa, J.; Shainy, F. Magnetic Titanium Dioxide Embedded Molecularly Imprinted Polymer Nanocomposite for the Degradation of Diuron under Visible Light. *React. Funct. Polym.* **2020**, *152*, 104597.
- (19) Lin, Q.; Unal, S.; Fornof, A. R.; Armentrout, R. S.; Long, T. E. Synthesis and Characterization of Telechelic Phosphine Oxide Polyesters and Cobalt(II) Chloride Complexes. *Polymer* **2006**, 47, 4085–4093.
- (20) Zhang, R.-C.; Sun, D.; Zhang, R.; Lin, W.-F.; Macias-Montero, M.; Patel, J.; Askari, S.; McDonald, C.; Mariotti, D.; Maguire, P. Gold Nanoparticle-Polymer Nanocomposites Synthesized by Room Temperature Atmospheric Pressure Plasma and Their Potential for Fuel Cell Electrocatalytic Application. *Sci. Rep.* 2017, 7, 46682.
- (21) Kuralay, F.; Erdem, A. Gold Nanoparticle/Polymer Nanocomposite for Highly Sensitive Drug-DNA Interaction. *Analyst* **2015**, 140, 2876–2880.
- (22) Ports, B. F.; Weiss, R. A. One-Step Melt Extrusion Process for Preparing Polyolefin/Clay Nanocomposites Using Natural Montmorillonite. *Ind. Eng. Chem. Res.* **2010**, *49*, 11896–11905.
- (23) Silva, R. D.; Chaparro, T. de C.; Monteiro, I. S.; Dugas, P.-Y.; D'Agosto, F.; Lansalot, M.; Martins dos Santos, A.; 'Bourgeat-Lami, E. Tailoring the Morphology of Polymer/Montmorillonite Hybrid Latexes by Surfactant-Free Emulsion Polymerization Mediated by Amphipathic MacroRAFT Agents. *Macromolecules* **2019**, *52*, 4979–4988.
- (24) Zandsalimi, K.; Akbari, B.; Mehrnejad, F.; Bagheri, R. Compatibilization of Clays and Hydrophobic Polymers: The Case of Montmorillonite and Polyetheretherketone. *Polym. Bull.* **2020**, *77*, 5505–5527
- (25) Dufresne, A. Cellulose Nanomaterial Reinforced Polymer Nanocomposites. *Curr. Opin. Colloid Interface Sci.*; Elsevier Ltd., 2017; pp 1–8.
- (26) Santos, F.; Bell, T.; Stevenson, A.; Christensen, D.; Pfau, M.; Nghiem, B.; Kasprzak, C.; Smith, T.; Fernando, R. Syneresis and Rheology Mechanisms of a Latex-HEUR Associative Thickener System. *J. Coatings Technol. Res.* **2017**, *14*, 57–67.
- (27) Ahmad, A.; Mubarak, N. M.; Naseem, K.; Tabassum, H.; Rizwan, M.; Najda, A.; Kashif, M.; Bin-Jumah, M.; Hussain, A.; Shaheen, A.; Abdel-Daim, M.; Ali, S.; Hussain, S. Recent Advance-

- ment and Development of Chitin and Chitosan-Based Nano-composite for Drug Delivery: Critical Approach to Clinical Research. *Arab. J. Chem.* **2020**, *13*, 8935–8964.
- (28) Hourston, D. J.; Romaine, J. Modification of Natural Rubber Latex. II. Natural Rubber Poly(Methyl Methacrylate) Composite Latexes Synthesized Using an Amine-activated Hydroperoxide. *J. Appl. Polym. Sci.* **1990**, 39, 1587–1594.
- (29) Ji, Y.; Marshall, J. E.; Terentjev, E. M. Nanoparticle-Liquid Crystalline Elastomer Composites. *Polymers* **2012**, *4*, 316–340.
- (30) Said, R. A. M.; Hasan, M. A.; Abdelzaher, A. M.; Abdel-Raoof, A. M. Review—Insights into the Developments of Nanocomposites for Its Processing and Application as Sensing Materials. *J. Electrochem. Soc.* **2020**, *167*, No. 037549.
- (31) Mauter, M. S.; Elimelech, M.; Osuji, C. O. Nanocomposites of Vertically Aligned Single-Walled Carbon Nanotubes by Magnetic Alignment and Polymerization of a Lyotropic Precursor. *ACS Nano* **2010**, *4*, 6651–6658.
- (32) Ahn, C. H.; Baek, Y.; Lee, C.; Kim, S. O.; Kim, S.; Lee, S.; Kim, S.-H.; Bae, S. S.; Park, J.; Yoon, J. Carbon Nanotube-Based Membranes: Fabrication and Application to Desalination. *J. Ind. Eng. Chem.* **2012**, *18*, 1551–1559.
- (33) Fu, F.; Wang, Q. Removal of Heavy Metal Ions from Wastewaters: A Review. J. Environ. Manage. 2011, 92, 407–418.
- (34) Kwon, N. K.; Kim, H.; Han, I. K.; Shin, T. J.; Lee, H. W.; Park, J.; Kim, S. Y. Enhanced Mechanical Properties of Polymer Nanocomposites Using Dopamine-Modified Polymers at Nanoparticle Surfaces in Very Low Molecular Weight Polymers. *ACS Macro Lett.* **2018**, *7*, 962–967.
- (35) Rafiee, M. A.; Rafiee, J.; Wang, Z.; Song, H.; Yu, Z. Z.; Koratkar, N. Enhanced Mechanical Properties of Nanocomposites at Low Graphene Content. *ACS Nano* **2009**, *3*, 3884–3890.
- (36) Wang, W.; Hou, G.; Zheng, Z.; Wang, L.; Liu, J.; Wu, Y.; Zhang, L.; Lyulin, A. V. Designing Polymer Nanocomposites with a Semi-Interpenetrating or Interpenetrating Network Structure: Toward Enhanced Mechanical Properties. *Phys. Chem. Chem. Phys.* **2017**, 19, 15808–15820.
- (37) Alison, L.; Menasce, S.; Bouville, F.; Tervoort, E.; Mattich, I.; Ofner, A.; Studart, A. R. 3D Printing of Sacrificial Templates into Hierarchical Porous Materials. *Sci. Rep.* **2019**, *9*, 409.
- (38) Wang, C.; Huang, W.; Zhou, Y.; He, L.; He, Z.; Chen, Z.; He, X.; Tian, S.; Liao, J.; Lu, B.; Wei, Y.; Wang, M. 3D Printing of Bone Tissue Engineering Scaffolds. *Bioact. Mater.* **2020**, *5*, 82–91.
- (39) Aduba, D. C.; Margaretta, E. D.; Marnot, A. E. C.; Heifferon, K. V.; Surbey, W. R.; Chartrain, N. A.; Whittington, A. R.; Long, T. E.; Williams, C. B. Vat Photopolymerization 3D Printing of Acid-Cleavable PEG-Methacrylate Networks for Biomaterial Applications. *Mater. Today Commun.* **2019**, *19*, 204–211.
- (40) Zou, Q.; Grottkau, B. E.; He, Z.; Shu, L.; Yang, L.; Ma, M.; Ye, C. Biofabrication of Valentine-Shaped Heart with a Composite Hydrogel and Sacrificial Material. *Mater. Sci. Eng., C* **2020**, *108*, 110205.
- (41) Park, S. A.; Lee, S. J.; Seok, J. M.; Lee, J. H.; Kim, W. D.; Kwon, I. K. Fabrication of 3D Printed PCL/PEG Polyblend Scaffold Using Rapid Prototyping System for Bone Tissue Engineering Application. *J. Bionic Eng.* **2018**, *15*, 435–442.
- (42) Herzberger, J.; Meenakshisundaram, V.; Williams, C. B.; Long, T. E. 3D Printing All-Aromatic Polyimides Using Stereolithographic 3D Printing of Polyamic Acid Salts. *ACS Macro Lett.* **2018**, *7*, 493–497.
- (43) Majima, T.; Schnabel, W.; Weber, W. Phenyl-2,4,6-trimethylbenzoylphosphinates as Water-soluble Photoinitiators. Generation and Reactivity of OP(C6H5)(O-) Radical Anions. *Die Makromol. Chemie* 1991, 192, 2307–2315.
- (44) Fairbanks, B. D.; Schwartz, M. P.; Bowman, C. N.; Anseth, K. S. Photoinitiated Polymerization of PEG-Diacrylate with Lithium Phenyl-2,4,6-Trimethylbenzoylphosphinate: Polymerization Rate and Cytocompatibility. *Biomaterials* **2009**, *30*, 6702–6707.

- (45) Jiang, T.; He, Y.; Jian, Y.; Nie, J. Exploration for Decreasing the Volume Shrinkage for Photopolymerization. Prog. Org. Coatings 2012, 75, 398-403.
- (46) Scott, P. J.; Kasprzak, C. R.; Feller, K. D.; Meenakshisundaram, V.; Williams, C. B.; Long, T. E. Light and Latex: Advances in the Photochemistry of Polymer Colloids. Polym. Chem. 2020, 11, 3498-3524.
- (47) Nguyen, A. K.; Goering, P. L.; Reipa, V.; Narayan, R. J. Toxicity and Photosensitizing Assessment of Gelatin Methacryloyl-Based Hydrogels Photoinitiated with Lithium Phenyl-2,4,6-Trimethylbenzoylphosphinate in Human Primary Renal Proximal Tubule Epithelial Cells. Biointerphases 2019, 14, No. 021007.
- (48) Hans-Jurgen, B.; Karlheinz, G.; Michael, K. Physics and Chemistry of Interfaces, 3rd ed.; Wiley-VCH: Weinham, 2013.
- (49) Szilagyi, I.; Trefalt, G.; Tiraferri, A.; Maroni, P.; Borkovec, M. Polyelectrolyte Adsorption, Interparticle Forces, and Colloidal Aggregation. Soft Matter 2014, 10, 2479.
- (50) Lan, Y.; Caciagli, A.; Guidetti, G.; Yu, Z.; Liu, J.; Johansen, V. E.; Kamp, M.; Abell, C.; Vignolini, S.; Scherman, O. A.; Eiser, E. Unexpected Stability of Aqueous Dispersions of Raspberry-like Colloids. Nat. Commun. 2018, 9, 3614.
- (51) Berardinelli, F. M.; Dolce, T. J.; Walling, C. Degradation and Stabilization of Polyacetal Copolymers. J. Appl. Polym. Sci. 1965, 9,
- (52) Ligon, S. C.; Liska, R.; Stampfl, J.; Gurr, M.; Mülhaupt, R. Polymers for 3D Printing and Customized Additive Manufacturing. Chem. Rev. 2017, 117, 10212-10290.
- (53) Jia, N.; Fraenkel, H. A.; Kagan, V. A. Effects of Moisture Conditioning Methods on Mechanical Properties of Injection Molded Nylon 6. J. Reinf. Plast. Compos. 2004, 23, 729-737.
- (54) Turner, D. T.; Schwartz, A. The Glass Transition Temperature of Poly(N-Vinyl Pyrrolidone) by Differential Scanning Calorimetry. Polymer 1985, 26, 757-762.
- (55) Ma, C.; Ji, T.; Robertson, C. G.; Rajeshbabu, R.; Zhu, J.; Dong, Y. Molecular Insight into the Mullins Effect: Irreversible Disentanglement of Polymer Chains Revealed by Molecular Dynamics Simulations. Phys. Chem. Chem. Phys. 2017, 19, 19468-19477.

□ Recommended by ACS

Additive Manufacturing of Hydrocarbon Elastomers via Simultaneous Chain Extension and Cross-linking of **Hydrogenated Polybutadiene**

Philip J. Scott, Timothy E. Long, et al.

FEBRUARY 01, 2019

ACS APPLIED POLYMER MATERIALS

RFAD 🗹

Supramolecular Salts for Additive Manufacturing of **Polyimides**

Clay B. Arrington, Timothy E. Long, et al.

SEPTEMBER 29, 2021

ACS APPLIED MATERIALS & INTERFACES

READ **C**

Bioderived 4D Printable Terpene Photopolymers from Limonene and β-Myrcene

Eric Constant, Andrew C. Weems, et al.

MAY 24, 2022

BIOMACROMOLECULES

RFAD 17

Linalool Derivatives for Natural Product-Based 4D Printing Resins

David Merckle, Andrew C. Weems, et al.

SEPTEMBER 02 2021

ACS SUSTAINABLE CHEMISTRY & ENGINEERING

READ **C**

Get More Suggestions >